DOI: https://doi.org/10.57233/ihcfs.029

ISBN: 978-978-68-07775

BOOK OF PROCEEDINGS

IHCFS – 2025 WEBSITE: fos.fugusau.edu.ng

FRACTIONAL DERIVATIVE UNSTEADY COUETTE-FLOW THROUGH COMPOSITE CHANNEL PARTIALLY FILLED WITH POROUS MATERIAL AND PARTIALLY WITH A CLEAR FLUID

Shehu A. Muhammad[1*]; Muhammad L. Kaurangini[2;] Falade K. Iyanda[3];
Kabir L. Yusuf[4]; Muhammad K. Musa[5].
[1] Mathematics Department, School of Basic and Remedial, Ahmadu Bello University, Zaria.
[2,3] Mathematics Department, Aliko Dangote University of Science and Technology, wudil
[4,5]Mathematics Department, Ahmadu Bello University, Zaria.
[1*]**Corresponding author's email Address:**shehukurami65@gmail.com.

ABSTRACT

This work examines unsteady Couette flow in a composite microchannel partially occupied by a porous medium and a clear fluid, using a fractional-order framework to account for memory effects. The Brinkman–extended Darcy equation models the porous region, while the Stokes equation describes the clear region. Governing equations are formulated with the Caputo–Fabrizio fractional derivative, transformed into the Laplace domain, and solved semi analytically. Time-domain solutions are obtained through Riemann-sum approximation and analyzed using MATLAB (2016). The study explores the influence of key parameters on velocity profiles, interfacial velocity, skin friction, and mass flux. Results indicate that transient and interfacial velocities, as well as mass flux, increase with time, whereas skin friction at the channel walls decreases. These findings highlight the effectiveness of fractional-order modelling in capturing nonlocal temporal effects in microscale flows through composite porous–clear structures.

Keywords: Unsteady Couette-Flow, Composite microchannel, Fractional.

NOMENCLATURE

u_f' Dimensional velocity in the clear fluid region.
u_p' Dimensional velocity in the porous medium region.
u_f Dimensionless velocity in the clear fluid region.
u_p Dimensionless velocity in the porous medium region.
U_i Interfacial velocity in dimensionless form.
y' Dimensional y coordinate.
y Dimensionless y coordinate.
ρ Density of the fluid.
β Stress jump coefficient.
Da Darcy number.
υ_f Kinematics viscosity of the fluid.
υ_e Effective kinematics viscosity of the fluid saturated porous material.
F Tangential momentum accommodation coefficient.
β_v Dimensionless variable.
Kn Kundsen number.
λ Molecular mean free path.
k Permeability of the porous material.
d Interfacial position.
u_{ti} Transient interfacial velocity.
u_t Transient velocity.
$\tau_{0,1,d}$ Skin friction at the wall of the porous medium.
$\tau_{11,d1}$ Skin friction at the wall of the clear fluid region.
α Fractional parameter.
Q_f Mass flux of the clear fluid.
Q_p Mass flux of the porous fluid.

1.0 INTRODUCTION

A fractional time derivative is a generalized mathematical operator that extends the concepts of differentiation D and integration J. While the classical operators $\left(Df(x) = \frac{d}{dx}f(x)\ and\ Jf(x) = \int_0^x f(s)ds.\right)$ describe integer-order differentiation and integration, the fractional derivative allows these operators to assume real or complex powers. This generalization enables the modelling of dynamic systems with greater accuracy, particularly those exhibiting memory and hereditary effects.

DOI: https://doi.org/10.57233/ihcfs.029

ISBN: 978-978-68-07775

BOOK OF PROCEEDINGS

IHCFS – 2025 WEBSITE: fos.fugusau.edu.ng

Generalized Couette flow refers to the flow generated by the combined influence of an imposed pressure gradient and the impulsive motion of one of the confining plates. The study of fluid transport through composite microchannels—partially filled with porous materials and partially with clear fluids—has gained increasing attention due to its broad applications in engineering and science. These include biomedical systems, separation processes in chemical industries, dispersion of contaminants in saturated soils, and crude oil recovery. The rapid development of microfluidic devices has further motivated extensive investigations into such flow systems.

For example, Michael *et al*. (2022) studied unsteady generalized Couette flow in a horizontal channel subject to sudden application or removal of porous material, showing that the time to reach steady state, skin friction, and volumetric flow rate are strongly influenced by such abrupt changes. Ojemeri, and Onwubuya (2023) studied significance of viscous dissipation and porosity effects in a heated superhydrophobic microchannel. Find that Darcy (porosity) strongly influences the velocity, especially when viscous dissipation is significant; the superhydrophobic surface plays a strong role in flow behaviour. Also, Kumar et al. (2025) studied numerical investigation of heat transfer performance of a microchannel heat sink using porous media. They identify conditions (porosity, flow rate and nanofluid concentration) that optimize thermal performance.

Despite these significant contributions, most existing studies on Couette flow in composite channels have been restricted to classical integer-order models. Such models, while effective in capturing fundamental flow features, are often limited in representing memory and nonlocal effects that are inherent at microscale and in porous–clear fluid interactions. Fractional-order derivatives provide a powerful framework for overcoming these limitations by incorporating hereditary effects and long-range temporal dependencies into the governing equations. Moreover, very few investigations have addressed unsteady Couette flow in composite microchannels using fractional-order operators, particularly the Caputo–Fabrizio definition, which avoids singular kernels and offers improved physical applicability. This gap motivates the present work, which develops and analyzes a fractional-order model of unsteady Couette flow through a composite microchannel partially filled with a porous medium and partially with a clear fluid. The study aims to provide deeper insights into the transient behaviour of velocity, interfacial flow, skin friction, and mass flux under fractional dynamics.

2.0 MATHEMATICAL ANALYSIS

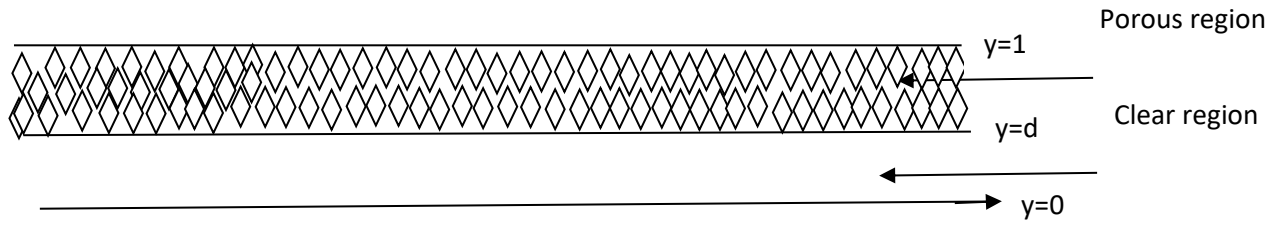

The figure above show the flow formation in an infinite horizontal parallel-plate.

At $t \leq 0$ both the plates and the fluid are at the same state. At $t > 0$, the lower plate is subjected to motion while the upper plate remains at rest. The middle plate is the interface between the porous fluid and the clear fluid regions.

Base on the above setup, the governing equations in dimensionless form for the fluid flow formation are as follows:

DOI: https://doi.org/10.57233/ihcfs.029

ISBN: 978-978-68-07775

BOOK OF PROCEEDINGS

$$\frac{\partial^{\alpha} u_f}{\partial t^{\alpha}} = \frac{\partial^2 u_f}{\partial y^2} \quad (1)$$

$$\frac{\partial^{\alpha} u_p}{\partial t^{\alpha}} = \gamma \frac{\partial^2 u_p}{\partial y^2} - \frac{u_p}{Da} \quad (2)$$

The non-dimensional parameters are as follows:

$$u_f = \frac{u_f'}{u},\ u_p = \frac{u_p'}{u},\ y = \frac{y'}{h'} \quad d = \frac{d'}{h'}\ \ y = \frac{t'\nu}{h^2}$$
$$\gamma = \frac{\nu_e}{\nu_p} \quad Da = \frac{k'}{h^2}\beta_v = \frac{2-F}{F} \quad (3)$$

The Initial and boundary condition are:

$$t \le 0:\ u_f = 1 + \beta_v Kn \frac{\partial u_f}{\partial y} aty = 0$$
$$\mathrm{u_f = u_p},\quad \gamma \frac{\partial u_f}{\partial y} - \frac{\partial u_p}{\partial y} = \frac{\beta_v}{\sqrt{Da}} u_i aty = d$$
$$u_p = -\beta_v Kn \frac{\partial u_p}{\partial y} aty = 1 \quad (4)$$
$$u_i = u_p = u_f,\quad \frac{\partial u_p}{\partial y} - \frac{\partial u_f}{\partial y} = \frac{\beta_v}{\sqrt{Da}} u_i aty = d$$

Caputo-Fabrizio definition (method) of solving fractional derivatives is used to the equations, as used in Ridwan et al (2022), as follows:

$$\{D_t^{\alpha} f(x,t)\} = \frac{su(x,q) - u(x,0)}{s(1-\alpha) + \alpha}$$

Now, applying Laplace transformation techniques and using Caputo-Fabrizio definition as stated above to (1) and (2), become:

$$\frac{d^2\bar{u_f}}{dy^2} - \left(\frac{as}{s+b}\right)\bar{u}_f = 0 \quad (5)$$

$$\frac{d^2 u_p}{dy^2} - \frac{1}{\gamma}\left(\frac{1}{Da} + \frac{as}{s+b}\right)u_p = 0 \quad (6)$$

Using the initial and boundary conditions in equation (4) above, Equations (5) and (6) are solved as follows:

$$\bar{u}_f(y,s) = C_1 \cosh(Ay) + C_2 \sinh(Ay) \quad \text{and} \quad \bar{u}_p(y,s) = C_3 \cosh(By) + C_4 \sinh(By) \quad (7)$$

$$\text{where: A} = \sqrt{\frac{as}{s+b}}\ ;\ \text{B} = \sqrt{\frac{1}{\gamma}\left(\frac{1}{Da} - \frac{as}{s+b}\right)};\ c_1 = \frac{1}{s}\left[1 - \frac{\beta_v k_n}{a_1}\cosh(Ad)\right] + \frac{A\beta_v k_n u_i}{a_1};$$
$$c_2 = \frac{1}{a_1}\left[u_i - \frac{1}{s}\cosh(Ad)\right];\ c_3 = -\frac{u_i a_3}{a_4}\ ;\ c_4 = \frac{u_i a_2}{a_4} \quad (8)$$

At the interface,

$$\gamma \frac{du_p}{dy} - \frac{du_f}{dy} = \frac{\beta}{\sqrt{Da}} U_i \qquad At\ y = d \quad (9)$$

Differentiating equations (7) $At\ y = d$ these gives:

$$\frac{d\bar{u_f}}{dy} = A[c_1 \sinh(Ad) + c_2 \cosh(\mathrm{Ad})] \text{and} \frac{d\bar{u_p}}{dy} = \gamma B[c_3 \sinh(Bd) + c_4 \cosh(\mathrm{Bd})] \quad (10)$$

By substituting equations (10), thanequation (9) is solved to give:

$$U_i = \frac{Ax_1 \sinh(Ad) - \frac{1}{sa_1}cosh^2(Ad)}{\frac{\gamma B}{a_4}[a_2 \cosh(Ad) - a_3 \sinh(Ad)] - \frac{A}{a_1}[A\beta_v k_n \sinh(Ad) + \cosh(Ad)] - \frac{\beta}{\sqrt{Da}}} \quad (11)$$

$$\text{Where: } a_1 = \sinh(Ad) + \beta_v k_n \cosh(Ad)\ ;\ a_2 = \beta_v k_n \mathrm{B} \sinh(B) + \cosh(B)$$
$$a_3 = \sinh(B) + \beta_v k_n B \cosh(B)\ ;\ a_4 = a_2 \sinh(Bd) - a_3 \cosh(Bd)$$
$$x_1 = \frac{1}{s}\left(1 - \frac{A\beta_v}{a_1}\cosh(Ad)\right) \quad (12)$$

DOI: https://doi.org/10.57233/ihcfs.029

ISBN: 978-978-68-07775

BOOK OF PROCEEDINGS

3.0 STEADY STATE

In microchannel flows, the steady state refers to the condition where the fluid motion becomes independent of time, and flow variables remain constant. However, this regime is not attained immediately; the fluid initially undergoes a transient state, during which velocity and other flow properties evolve with time until equilibrium is reached. Once the transient effects diminish, the system approaches a steady state, characterized by a constant and uniform flow through the microchannel.

To determine the steady, we set $\frac{\partial^{\alpha} u_p}{\partial t^{\alpha}} = \frac{\partial^{\alpha} u_p}{\partial t^{\alpha}} = 0$ from equations (1) and (2) so that

$$\frac{d^2 \bar{u_f}}{dy^2} = 0 \qquad (13)$$

$$\gamma \frac{d^2 u_p}{dy^2} - \frac{u_p}{Da} = 0 \qquad (14)$$

Equation (13) is integrated twice to give:

$$\bar{u}_f(y) = Ay + B \qquad (15)$$

and equation (14) is solved to give

$$\bar{u}_p(y) = F_1 \cosh(Dy) + F_2 \sinh(Dy) \qquad (16)$$

Where the values of the constants are:

$$\left.\begin{array}{l} D = \frac{1}{\sqrt{\gamma Da}}; F_1 = \frac{U_i x_3}{x_4}; F_2 = \frac{U_i x_2}{x_4}; A = \frac{u_i - 1}{d + \beta_v k_n}; B = 1 + \beta_v k_n \left(\frac{u_i - 1}{d + \beta_v k_n}\right) \\ x_2 = \beta_v k_n \sinh(D) + \cosh(D); \; x_3 = \sinh(D) + \beta_v k_n \cosh(D) \; ; \\ x_4 = x_3 \sinh(Dd) + x_2 \cosh(Dd) \end{array}\right\} \qquad (17)$$

At the interface,

$$\gamma \frac{d\bar{u}_p}{dy} - \frac{d\bar{u}_f}{dy} = \frac{\beta}{\sqrt{Da}} U_i \qquad At\ y = d \qquad (18)$$

Differentiating equations (15) and (16) gives:

$$\frac{d\bar{u}_f}{dy} = A \quad and \quad \frac{d\bar{u}_p}{dy} = D[F_1 \sinh(Dd) + F_2 \cosh(Dd) \qquad (19)$$

By substituting equations (19) into equation (18) which is solved to give:

$$u_i = \frac{1}{(d + \beta_v k_n)\left[\frac{\gamma D}{x_4}(x_3 \sinh(Dd) - x_2 \cosh(Dd)) - \left(\frac{1}{d + \beta_v k_n} + \frac{\beta}{\sqrt{Da}}\right)\right]} \qquad (20)$$

$Where\ x_2;\ x_3; x_4$ are as defined in equation (17) above.

4.0 SKIN FRICTION (Transient State)

As the fluid flows through the channel, frictional force (skin friction)atthe interface between fluid and immediate channel surface intends to impede forward movement of the plate occurs. The skin friction is the derivative of the solutions of the velocity and is given as follows:

$$\left.\frac{d\bar{u}_f}{dy}\right|_{y=-0,\ y=d} = A[C_1 \sinh(Ay) + C_2 \cosh(Ay)] \text{ and } \left.\frac{d\bar{u_p}}{dy}\right|_{y=-1,\ y=d} = B[C_3 \sinh(By) + C_4 \cosh(By)] \qquad (21)$$

The skin frictions are:

$$\bar{\tau}_0 = AC_2 \quad ; \quad \bar{\tau}_d = A[C_1 \sinh(Ad) + C_2 \cosh(Ad)] \qquad (22) \text{ And}$$

$$\bar{\tau}_1 = B[C_3 \sinh(B) + C_4 \cosh(B)] \quad ; \bar{\tau}_d = B[C_3 \sinh(Bd) + C_4 \cosh(Bd)]$$

(23)$Where\ A, B, C_1, C_2, C_3, C_4$ are constants as defined above.

5.0 MASS FLUX (Transient State)

The volume of the fluid that flows through the channel per unit area (Mass flow rate or mass flux) is also calculated and is given as:

$$Q_f(y) = \int_0^d (c_1 \cosh(Ay) + c_2 \sinh(Ay))dy \text{ and } Q_p(y) = \int_d^1 (c_3 \cosh(By) + c_4 \sinh(By))dy \qquad (24)$$

DOI: https://doi.org/10.57233/ihcfs.029

ISBN: 978-978-68-07775

BOOK OF PROCEEDINGS

Equations (24) are solved to give:

$Q_f = \frac{1}{A}[c_1 \sinh(Ad) + c_2(\cosh(Ad) - 1)]$ (25)

$Q_p = \frac{1}{B}[c_3(\sinh(B) + \sinh(Bd)) + c_4(\cosh(B) - \cosh(\mathrm{Bd}))]$ (26)

$Q = Q_f + Q_p$

$Q = \frac{1}{A}[c_1 \sinh(Ad) + c_2(\cosh(Ad) - 1)] + \frac{1}{B}[c_3(\sinh(B) + \sinh(Bd)) + c_4(\cosh(B) - \cosh(\mathrm{Bd}))]$ (27)

6.0 SKIN FRICTION (STEADY STATE)

The skin frictions of the steady state are the derivatives of the integral of the solutions of the equations of the steady state.

$\left.\frac{d\bar{u}_f}{dy}\right|_{y=0,\ y=d} = Ay + B$ and $\left.\frac{du_p}{dy}\right|_{y=1,\ y=d} = \frac{1}{D}[F_1 \sinh(Dy) + F_2 \cosh(Dy)]$ (28)

The skin friction ofthe Steady State are:

$\tau_0 = A;\ \tau_d = A$(29)

And

$\tau_d = \frac{1}{D}[F_1 \sinh(Dd) + F_2 \cosh(Dd)]$; $\tau_1 = \frac{1}{D}[F_1 \sinh(D) + F_2 \cosh(D)]$ (30)

$Where\ A, D, F_1, F_2$ are constants.

7.0 MASS FLUX (STEADY STATE)

The mass flux of the steady state is the integral of the solutions of the steady state, that is:

$Q_{sf} = \int_0^d (Ay + B)\, dy$ and $Q_{sp} = \int_d^1 (F_1 \cosh(Dy) + F_2 \sinh(Dy))\, dy$ (31)

Equations (31) are solved as:

$Q_{f\ s.s} = \frac{Ad^2}{2} + Bd$ (32)

$Q_{p\ s.s} = \frac{1}{D}[F_1(\sinh(D) - \sinh(Dd)) + F_2(\cosh(D) - \cosh(Dd))]$ (33)$Q = Q_{sf} + Q_{sp}$

$Q_{s.s} = \frac{Ad^2}{2} + Bd + \frac{1}{D}[F_1(\sinh(D) - \sinh(Dd)) + F_2(\cosh(D) - \cosh(Dd))]$ (34)

It can be observed that the expressions for transient states velocities, as well as the resulting calculated expressions for skin friction and volumetric mass flow rate are all in Laplace domain. To derive the corresponding time domain form of these equations appear to be complex. Hence a numerical method base on the Riemann-Sum Approximation Method as used by Jha et al (2023) and Isa [17] is employed. This approach requires that the Laplace inverse of any function $\bar{w}(y, p)$ can be obtained from:

$w(y,t) = \frac{e^{\varepsilon t}}{t}\left[\frac{1}{2}\bar{w}(y,\varepsilon) + Re\sum_{k=1}^{n}\bar{w}\left(y, \varepsilon + \frac{ik\pi}{t}\right)(-1)^k\right]$(42)

Where Re is the real part of the expression, $i = \sqrt{-1}$ is the imaginary number and n is the number of iteration used while ε is the real part of Bromwich contour used for inverting a function from Laplace domain to its corresponding time domain. If the number of iteration most be minimized and faster convergence is to be achieved, then the product $\varepsilon t = 4.7$. Appropriate substitutions will yield the corresponding Laplace inverses for the temperature, share stress, rate of heat transfer and volumetric mass flow rate.

DOI: https://doi.org/10.57233/ihcfs.029

ISBN: 978-978-68-07775

BOOK OF PROCEEDINGS

IHCFS – 2025 WEBSITE: fos.fugusau.edu.ng

8.0 RESULT AND DISCUSSIONS

This section presents and analyzes the analytical results for unsteady Couette flow in a composite microchannel partially occupied by a porous medium and a clear fluid. The governing equations were solved analytically, and numerical computations were performed using MATLAB (2016). The outcomes are illustrated through line graphs depicting the evolution of transient velocity, interfacial velocity, skin friction (both transient and steady-state), and mass flux under varying system parameters, including the Darcy number (Da), porous-layer thickness (d), slip parameter (β), position (y), and fractional order(α).

The findings highlight the coupled influence of porous permeability, slip effects, layer thickness, and fractional-order memory on velocity distribution, wall shear stress, and transport characteristics. Time is shown to be a critical factor governing flow evolution, with velocity and mass flux increasing monotonically, while skin friction decreases as the system approaches steady state.

These results provide valuable insights for the optimization of microscale transport processes in layered porous structures. In particular, they have practical relevance for the design of lab-on-chip devices, biofluidic systems, and porous filtration technologies, where precise control of velocity profiles, shear stresses, and flow rates is essential.

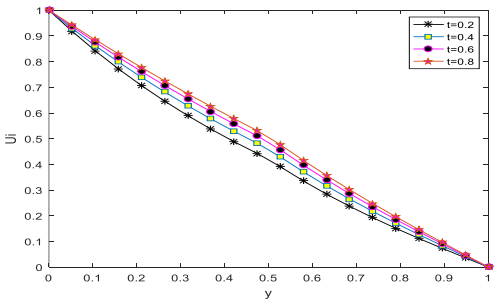

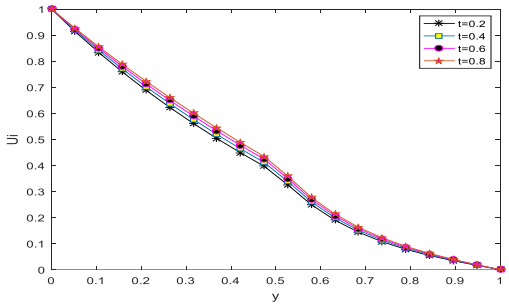

Fig1(a): Transient velocity profiles for different values of $tandy$ with $(Da = 1.0\ \gamma = 0.7; d = 0.5; \beta = 0.01, \alpha = 0.7)$.

Fig 1(b): Transient velocity profiles for different values of $t\ and\ y$ with$(Da = 0.1;\ \gamma = 0.5; d = 0.5;\ \beta = 0.01; \alpha = 0.5)$.

Figures $1(a) - 1(c)$ illustrate the transient velocity distributions for different Darcy numbers $(Da)$and time t, along the spatial coordinate y. In Figure $1(a)(Da = 1.0,\ \gamma = 0.7)$ and Figure $1(b)(Da = 0.1)$, the velocity increases with time, consistent with the physical expectation that the fluid accelerates from rest under the imposed shear. However, in Figure 1(c) $(Da = 0.01)$, the development of the velocity field is significantly slower, as the reduced permeability of the porous medium suppresses fluid motion near the interface. Across all cases, the velocity increment diminishes with time, signifying a gradual transition from transient to steady state. This asymptotic approach to equilibrium highlights the dominant role of permeability: lower Da values impose greater resistance, thereby retarding flow development, particularly near the porous–clear interface.

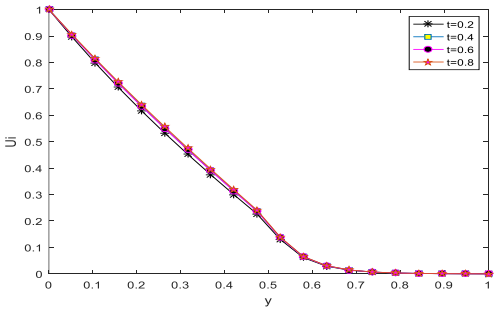

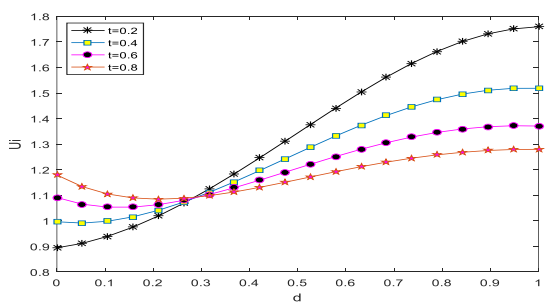

DOI: https://doi.org/10.57233/ihcfs.029

ISBN: 978-978-68-07775

BOOK OF PROCEEDINGS

IHCFS – 2025 WEBSITE: fos.fugusau.edu.ng

Fig1(c): Transient velocity profiles for different values ofFig .2(a): Interfacial velocity profiles for different values of
$t\ and\ y$ with $(Da = 0.01;\ \gamma = 0.5; d = 0.5;\ \beta = 0.0, \alpha = 0.7).t\ and\ d$ with $(Da = 1.0;\ \gamma = 0.5;\ \beta = -0.5, y = 0.5\ and \alpha = 0.5)$.

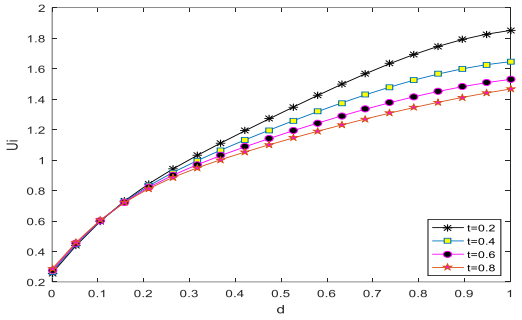

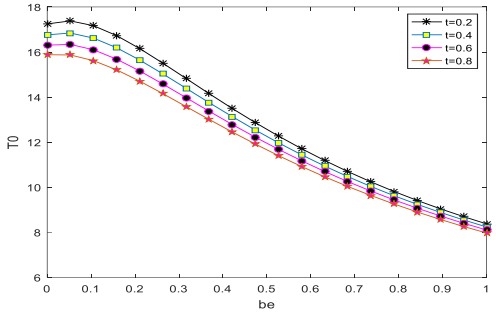

Fig2(b): Interfacial velocity profiles for different values of the velocity with different values of
$t\ and\ d$ with $(Da = 0.1;\ \gamma = 0.5;\ \beta = -0.5, y = 0.5\ and \alpha = 0.5).t\ and\ \beta$ with $(\mathrm{Da} = 1.0, \mathrm{y} = 1.0, \gamma = 0.5, \mathrm{d} = 0.1\ \mathrm{and}\ \alpha = 0.7)$.

Fig 3(a): Skin friction τ_0 of the velocity with different values of

Figures $2(a)$ and $2(b)$ present the interfacial velocity for varying times and porous thicknesses(d), with fixed $\beta = -0.5$ and $\gamma = 0.5$.For$Da = 1.0$, the interfacial velocity rises initially but stabilizes once transient effects subside, reflecting equilibrium between shear forces in the two regions. Conversely, for$Da = 0.1$, the interfacial velocity decreases due to lower permeability, which enhances resistance in the porous medium and reduces momentum transfer to the interface. The comparison demonstrates that interfacial dynamics are strongly governed by porous resistance, with lower Da values suppressing interface motion.

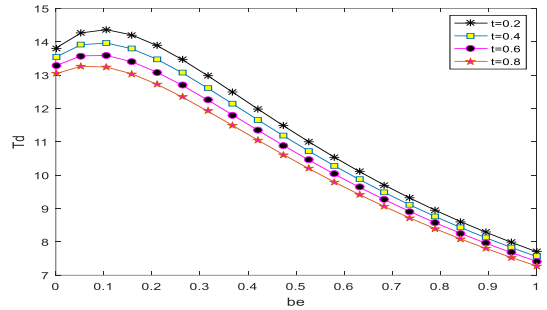

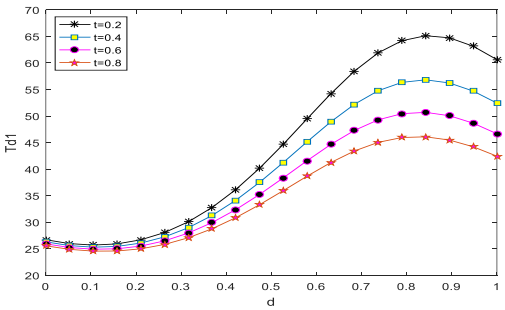

Fig3(b): Skin friction τ_d of the velocity with different values ofFig 3(c): Skin friction τ_{d1} of the velocity with different values of
t and β with $(\mathrm{Da} = 0.1, \gamma = 0.5, \mathrm{y} = 1.0, \mathrm{d} = 0.1 \mathrm{and}\ \alpha = 0.7)$. $t\ and\ d$ with $(\mathrm{Da} = 1.0, \gamma = 0.5, \beta = 0.5, \mathrm{y} = 0.5, \mathrm{and}\ \alpha = 0.7)$.

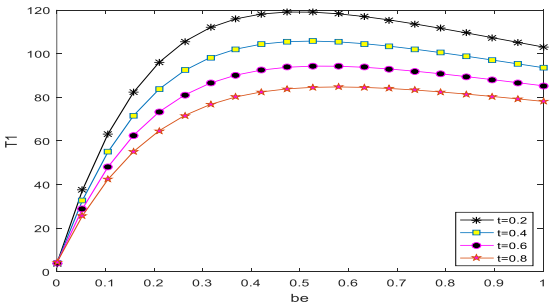

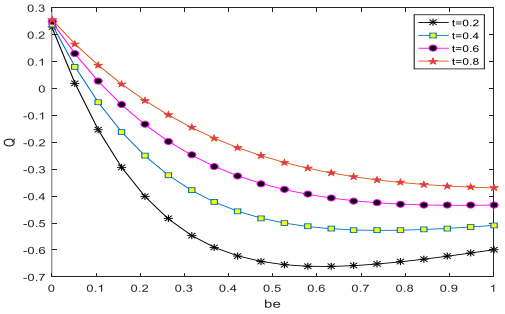

DOI: https://doi.org/10.57233/ihcfs.029

ISBN: 978-978-68-07775

BOOK OF PROCEEDINGS

IHCFS – 2025 WEBSITE: fos.fugusau.edu.ng

Fig3(d): Skin friction τ_1 of the velocity with different values of $t\ and\ \beta$ with $(\mathrm{Da} = 1.0, \gamma = 0.5, d = 0.1, \mathrm{y} = 0.5,\ \mathrm{and} \alpha = 0.7)$.

Fig 4(a): Mass flux profiles for the velocity with different values of $t\ and\ \beta$ with $(\mathrm{Da} = 1.0, \gamma = 0.5, \mathrm{y} = 1.0,\ \mathrm{d} = 0.2\ \mathrm{and}\ \alpha = 0.5)$.

Figures 3(a)–3(d) depict skin friction profiles in both the clear and porous regions under transient conditions. In the clear region, skin friction (τ_0, τ_d) decreases monotonically with time, indicating relaxation of velocity gradients at the fluid–wall boundary as the flow stabilizes. Higher slip parameter (β) values further reduce wall shear by weakening velocity gradients. In the porous region, similar decay trends are observed for τ_{d1}, confirming that shear stress in porous boundaries also relaxes with time. These results collectively demonstrate the tendency of both regions to approach shear equilibrium, with the transient state characterized by rapid initial decay followed by stabilization.

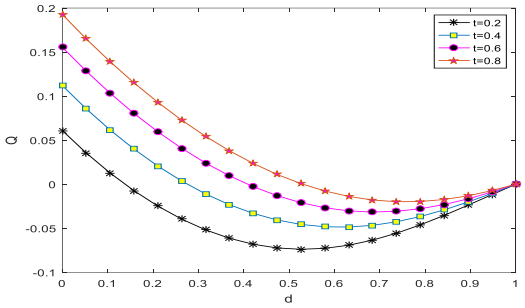

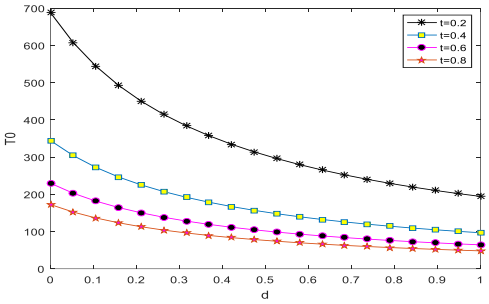

Fig4(b): Mass flux profiles for the velocity with different values of $t\ and\ d$ with $(\mathrm{Da} = 1.0, \gamma = 1.0, \mathrm{y} = 1.5,\ \beta = 0.5\ \mathrm{and}\ \alpha = 0.5)$.

Fig 5(a): Is the skin friction τ_0 of the steady state with different values of $t\ and\ d$ with $(\mathrm{Da} = 1.0, \gamma = 0.5, \beta = -0.4, \mathrm{y} = 0{,}5,\ \mathrm{and}\ \alpha = 0.5)$.

Figures $4(a)$ and $4(b)$ illustrate mass flux evolution with time under varying β and$d$. In both cases, mass flux increases monotonically, consistent with progressive flow development. Higher slip enhances mass flux by reducing drag at the boundary, while thinner porous layers promote greater transport by lowering hydraulic resistance.

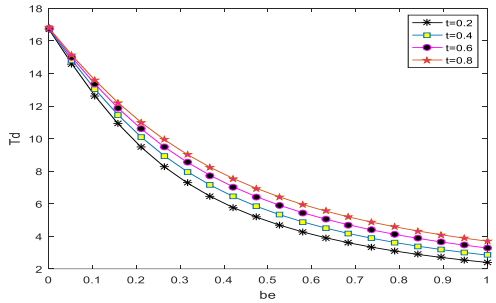

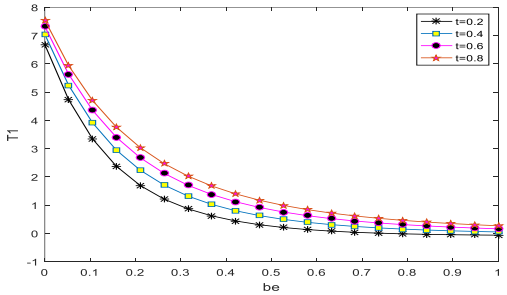

Fig5(b): shows the skin friction τ_d of the steady state with different values of $t\ and\ \beta$ with $(\mathrm{Da} = 1.0, \gamma = 0.5, d = 0.01, \mathrm{y} = 1.0,\ \mathrm{and}\ \alpha = 0.9)$.

Fig 5(c): Skin friction τ_1 of the steady state with different values of $t\ and\ \beta$ with $(\mathrm{Da} = 1.0, \gamma = 1.0, d = 0.2, \mathrm{y} = 1.0,\ \mathrm{and}\ \alpha = 0.9)$.

Figures 5(a)–5(d) present steady-state skin friction at different boundaries. In the clear region, skin friction at the lower wall decreases with time and porous thickness, reflecting reduced wall shear in fully developed flows. In contrast, skin friction at the upper wall increases with

DOI: https://doi.org/10.57233/ihcfs.029

ISBN: 978-978-68-07775

BOOK OF PROCEEDINGS

time, likely due to intensified shear gradients associated with slip effects. Within the porous region, shear dynamics show opposite trends: τ_1 increases with time, while τ_{d1} decreases. These contrasting behaviors emphasize the spatial variability of shear stress distribution, shaped by both flow development and material properties.

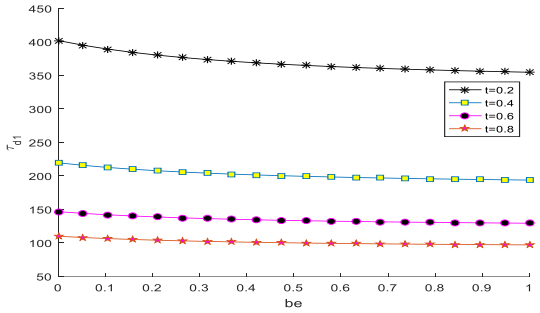

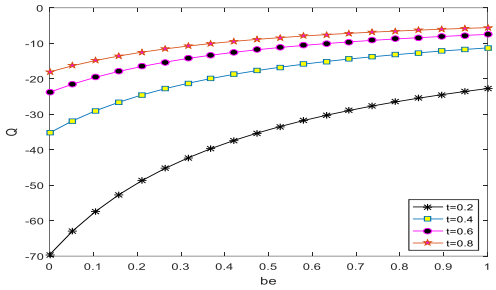

Fig5(d): shows the skin friction τ_{d1} of the steady state with different values ofFig 6(a): Mass flux of the steady state for different values of $t\ and\ \beta$ with $(\mathrm{Da} = 0.01, \gamma = 0.5, p = 0.2, d = 0.5, \mathrm{y} = 0.5,\ \mathrm{and}\ \alpha = 0.5)$. $t\ and\ \beta$ with (Da=1.0,$\gamma = 1.0, \mathrm{d} = 0.5 y = 1.0, \mathrm{and}\ \alpha = 0.5$).

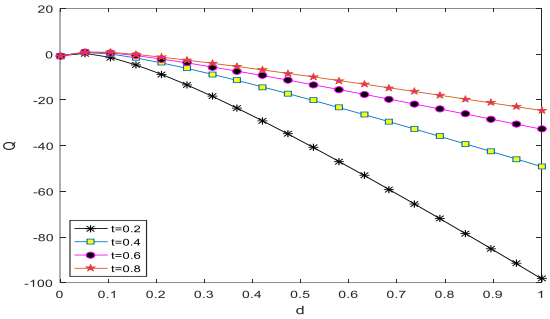

Fig.6(b): Mass flux of the steady state for different values of $tandd$ with (Da=0.01,$\gamma = 0.5, \beta = 0.4, y = 1.0, \mathrm{and}\ \alpha = 0.9$).

Finally, Figures 6(a) and 6(b) depict steady-state mass flux variations. In both cases, mass flux increases with time as the velocity field stabilizes. The role of slip is evident, as higher βvalues enhance transport by lowering boundary drag, while smaller d values (thinner porous layers) yield greater flux due to reduced flow resistance.

Overall, the results demonstrate that system behavior is strongly influenced by Darcy number, porous thickness, slip parameter, and fractional-order dynamics. Lower permeability slows velocity development and reduces interfacial motion, while slip effects enhance both velocity and mass transport. Skin friction generally decays with time in both regions, though its spatial distribution differs between clear and porous domains. Time evolution is central across all quantities, with velocity and flux increasing monotonically while wall shear relaxes toward equilibrium. These findings extend the earlier works by incorporating fractional-order dynamics, which capture memory effects absent in classical models. Consequently, the study provides deeper insights into transient and steady-state transport in layered porous microchannels. Such understanding is particularly valuable for the design and optimization of microscale transport systems—including lab-on-chip devices, bio-fluidic systems, and porous filtration technologies—where precise control of flow resistance, shear stress, and transport efficiency is essential.

DOI: https://doi.org/10.57233/ihcfs.029

ISBN: 978-978-68-07775

BOOK OF PROCEEDINGS

IHCFS – 2025 WEBSITE: fos.fugusau.edu.ng

9.0 VALIDATION OF RESULTS

A critical step in ensuring the reliability of the present analytical framework is the validation of numerical approximations against exact steady-state solutions. Table 1 presents a comparison of velocity profiles obtained using the Riemann-sum approximation (RSA) for both fractional and classical derivatives with the corresponding exact solutions. Across all spatial positions y, the differences between RSA and exact values are negligible, confirming the accuracy and stability of the adopted Laplace inversion procedure.

TABLE1: COMPARISON OF VELOCITY PROFILES

Y	Rieman-Sum Approximation Fractional Derivative	Rieman-Sum Approximation Classical Derivative	Exact Solution	Difference of (RSA &Exact) Fractional D.	Difference of (RSA &Exact) Classical D.
0.2	0.6586	0.6592	0.6592	-0.0006	0.0000
0.4	0.5732	0.5732	0.5732	0.0000	0.0000
0.6	0.4879	0.4878	0.4878	0.0001	0.0000
0.8	0.3799	0.3799	0.3799	0.0000	0.0000
1.0	0.2959	0.2959	0.2959	0.0000	0.0000

9.2 SKIN FRICTION VALIDATION (Upper and Lower Plates)

Further validation is provided through the analysis of skin friction at the upper (τ_1) and lower (τ_0) plates, summarized in Tables 2 and 3. The results reveal excellent agreement between fractional and classical formulations, with only minor deviations. A notable discrepancy occurs for τ_0 at $y = 0.2$, where a difference of -0.1557 indicates enhanced memory effects at earlier times or near-wall regions. However, this difference diminishes rapidly at higher spatial positions, reflecting convergence toward the classical limit as time progresses.

TABLE 2: SKIN FRICTION OF THE UPPER PLATE (τ_1)

Y	Rieman-Sum Approximation Fractional Derivative	Rieman-Sum Approximation Classical Derivative	Difference Between (Fractional & Classical Der.)
0.2	13.1065	13.0443	0.0622
0.4	12.5123	12.5123	0.0000
0.6	9.1433	9.1451	-0.0018
0.8	7.2604	7.2613	-0.0009
1.0	6.0674	6.0678	-0.0004

TABLE 3: SKIN FRICTION OF THE LOWER PLATE (τ_0)

Y	Rieman-Sum Approximation Fractional Derivative	Rieman-Sum Approximation Classical Derivative	Difference Between (Fractional & Classical Der.)
0.2	3.9510	4.1067	-0.1557
0.4	62.7963	62.7968	-0.0005
0.6	39.1992	39.1034	0.0958
0.8	26.1433	26.0727	0.0706
1.0	18.6577	18.6100	0.0477

Overall, the validation generally confirms that transient solutions asymptotically approach steady-state values at large times, in agreement with physical expectations.

DOI: https://doi.org/10.57233/ihcfs.029

ISBN: 978-978-68-07775

BOOK OF PROCEEDINGS

Furthermore, the skin friction profiles exhibit strong consistency between fractional and classical models, with minimal numerical deviations. In addition, the Riemann-sum approximation provides a robust and reliable scheme for Laplace-domain inversion in fractional-order fluid flow systems.

Thus, these results not only reinforce confidence in the present methodology but also demonstrate the effectiveness of fractional calculus in capturing transient memory effects in microchannel flows with composite porous structures.

10.0 CONCLUSION

This study highlights the applicability of fractional calculus in capturing transient flow dynamics within composite microchannels comprising porous and clear fluid regions. The main findings can be summarized as follows:

1. The fractional-order framework, particularly the Caputo–Fabrizio derivative, effectively incorporates memory and non-local effects, offering a more realistic representation than classical integer-order models.
2. Both bulk and interfacial velocities exhibit temporal growth, reflecting the progressive development of flow from an initial rest state toward equilibrium under imposed boundary and interfacial conditions.
3. Skin friction at channel walls decreases with time in both clear and porous domains, signifying boundary-layer development and gradual stabilization of shear stresses.
4. The volumetric flow rate increases as the system evolves, demonstrating enhanced transport capacity as unsteady flow approaches steady-state conditions.
5. Validation against analytical steady-state solutions confirms the accuracy of the Riemann-sum approximation and reinforces the robustness of the fractional modelling approach.

Overall, the results establish fractional calculus as a powerful tool for modelling unsteady microchannel flows, particularly in heterogeneous geometries where classical models fall short.

REFERENCES

Arif, M., Ali, F., Khan, I., & Nasir, K. S. (2020). A time fractional model with non-singular kernel: The generalized Couette flow of couple stress nanofluid. *IEEE Access, 8*, 77378–77395. https://doi.org/10.1109/ACCESS.2020.2989184

Jha, B. K., & Gambo, D. (2021). Role of exponentially decaying/growing time-dependent pressure gradient on unsteady Dean flow: A Riemann-sum approximation approach. *Arab Journal of Basic and Applied Sciences, 28*(1), 1–10. https://doi.org/10.1080/25765299.2021.1877644

Jha, B. K., Taiwo, S. Y., & Gambo, D. (2022). Transient Taylor Dean flow in a composite annulus with porous walls partially filled with porous material. *Journal of the Egyptian Mathematical Society, 30*(2), 1–12. https://doi.org/10.1186/s42787-022-00165-9

Jha, B. K., Musa, M. K., & Yusuf, L. K. (2023). Time-dependent pressure driven flow in a horizontal cylinder filled with a bidisperse porous material. *Heat Transfer, 52*(6), 1–15. https://doi.org/10.1002/htj.22808

Kumar et al, (2025). Numerical investigation of heat transfer performance of a microchannel heat sink using porous media. *Journal of Thermal Engineering (J Ther Eng),* vol. 11, No1, pp 141-158, 2025, Doi:10.14744/thermal.0000909.

Michael, A., Joseph, D., & Samuel, P. (2022). Unsteady generalized Couette flow in a horizontal channel with sudden application or removal of porous material. *Contemporary Mathematics, 3*(2). https://doi.org/10.37256/cm.322022.365

Ojemeri, G. and Onwubuya, I. O. (2023). Significance of viscous dissipation and porosity effects in a heated

superhydrphobicmicrochannel. *Journal of Engineering and Technology (JET), 2023.*

Ridwan, M., Ali, F., Khan, I., & Sheikh, N. A. (2022). Analytical solution for impact of Caputo–Fabrizio fractional derivative on MHD Casson fluid with thermal radiation and chemical reaction effects. *Fractal and Fractional, 6*(1), 38. https://doi.org/10.3390/fractalfract6010038

Sanjeeva, K. S., & Vineet, K. V. (2020). Exact solution of flow in a composite porous channel. *Archives of Mechanical Engineering, 67*(1), 1–15. https://doi.org/10.24425/ame.2020.131686

Shankar, S., & Jeevan, L. (2022). Approximate solutions for solving some special functions of fractional calculus via Caputo–Fabrizio sense. *Nepal Journal of Mathematical Sciences, 3*(2), 71–80. https://doi.org/10.3126/njmathsci.v3i2.49203